ACS Sustainable Chemistry & Engineering

pubs.acs.org/journal/ascecg

Research Article

Chitosan–Chitin Nanocrystal Films from Lobster and Spider Crab: Properties and Environmental Sustainability

Rut Fernández-Marín, Amaia Morales, Xabier Erdocia, Maider Iturrondobeitia, Jalel Labidi,* and Erlantz Lizundia*

Cite This: *ACS Sustainable Chem. Eng.* 2024, 12, 10363–10375

Read Online

ACCESS | Metrics & More | Article Recommendations | Supporting Information

ABSTRACT: The valorization of chitinous biomass from underutilized renewable carbon feedstock offers alternative routes for bioproduct development, reducing our dependence on nonrenewable and nonbiodegradable materials composed of fossil carbon. This work utilizes crustacean waste consisting of inedible shells to isolate chitin and its derivatives, chitin nanocrystals and chitosan, from lobster (*Homarus gammarus*) and spider crab (*Maja squinado*) shells. Chitin nanocrystals (ChNCs) with a degree of acetylation >93% and crystallinity >90% were obtained by demineralization, deproteinization and acid-hydrolysis, while chitosan was obtained by chitin deacetylation. Free-standing chitosan/ChNCs films were then fabricated from lobster and spider crab after dissolution and casting using 1.5% v/v formic acid. Lobster-derived materials exhibited a good balance between UV-shielding ability, blocking >96% of UV-C and UV-B, while being transparent at visible wavelengths. Neat chitosan films are semiductile, with elongations at break >13% and Young's modulus values of 2.3 ± 0.7 and 3.4 ± 1.2 GPa for lobster and spider crab-derived chitosan, respectively. Besides, the incorporation of ChNCs increases the Young's modulus to 5.5 ± 0.8 GPa at 2 wt % for lobster-derived films. Life cycle assessment (LCA) was conducted to quantify the environmental impact of film production and identify process hotspots for future optimization. A carbon footprint of 79.8 kg CO_2 equiv·kg^{-1} is obtained for chitosan/ChNC films processed using a 100% renewable energy mix. Results demonstrate that lobster-derived materials are relevant contenders toward defossilization by developing renewable-carbon containing bioproducts with competitive performance against fossil-based materials due to their optical and mechanical properties, as well as their potential biodegradability.

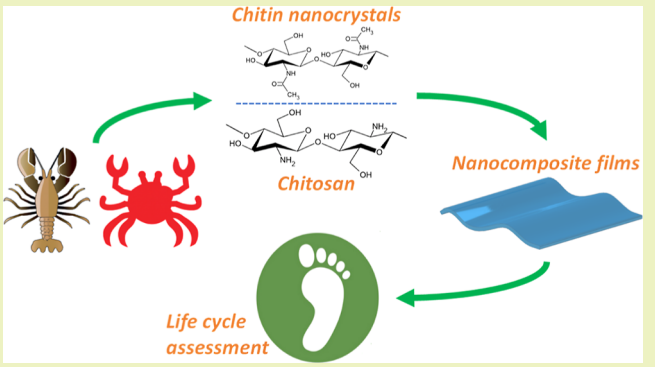

KEYWORDS: *chitosan, chitin nanocrystals, biopolymers, life cycle assessment, environmental sustainability*

1. INTRODUCTION

The linear use of fossil-derived materials remains at the core of the unprecedented global challenges that faces our society.[1−3] The growing population and rise in prosperity are accelerating the demand for materials. In this context, plastic production is projected to reach 1231 t annually by 2060, representing a threefold increase compared to the production in 2019.[4] The excessive use of nonrenewable plastics threatens resource availability and generates large amounts of durable waste that accumulates in an uncontrolled manner in terrestrial, river, or marine ecosystems. In this context, materials derived from renewable carbon feedstock can provide an environmentally sustainable and cost-effective alternative to conventional plastics.[5,6] The transition from the current linear fossil-based materials to circular biobased materials that rely on abundant, nontoxic, and renewable/biodegradable sources is attracting enormous attention.

Polysaccharides, polymeric carbohydrates, can balance the often self-exclusive attributes of renewability, biodegradability, and competitive functionalities, including processability, thermomechanical performance, and ease of functionalization.[7−9] Chitin, the second-most abundant natural polysaccharide on Earth and consisting of repeating $\beta(1,4)$-*N*-acetylglucosamine units, is becoming increasingly popular as an alternative to nonrenewable materials.[8,10,11] Chitin offers additional benefits in comparison to other biopolymers, which include structural strength and flexibility, hierarchical structure, and presence of acetyl groups and amino groups.[12] Chitin can be further modified to obtain chitin derivatives that show enhanced functionalities over the parent chitin polymer. In this context, chitin is partially deacetylated to produce chitosan, the

Received: February 9, 2024
Revised: May 29, 2024
Accepted: June 21, 2024
Published: June 28, 2024

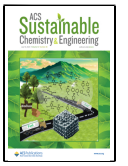

most important chitin derivative for various applications. Chitosan becomes soluble in aqueous acidic media at deacetylation degrees above 50%, making its process much easier. The cationic nature of chitosan, along with its processing ability, enables biomedical, cosmetic, agricultural, and food applications. In addition, chitin can be fibrillated down to obtain nanochitin, which consist of chitin nanocrystals or chitin nanofibrils. These colloidal entities possess outstanding mechanical and self-assembly properties,[8,10] making them useful in various technological applications as mechanical reinforcing material,[13] into biomimetic photonics,[11] packaging applications,[14] or battery electrolytes.[15]

Economically feasible methods for obtaining chitinous biomass typically involve controlled deconstruction of discarded crustacean shells. Crab endocuticles,[16] and shrimp shells,[17,18] have been the primary feedstock utilized for chitin valorization. However, there are still several chitinous sources that remain open to exploration for chitosan and chitin nanocrystal isolation. These sources may potentially result in larger yields or improved functionalities due to composition and morphology differences. For instance, lobster exoskeletons have a higher chitin content (20.3 wt %)[19] compared to *Maja squinado* spider crab (16 wt %).[20] Notwithstanding the clear environmental benefits that arise upon marine waste valorization,[21] which render materials containing renewable carbon, the use of acids as well as the need for large quantities of water and energy could endanger the overall sustainability of the material. These material and energy requirements can notably increase the embodied carbon, resulting in biobased materials with an increased CO_2 footprint. In this context, standardized and comparable procedures are necessary to quantify environmental impacts. The life cycle assessment (LCA) methodology conforms to ISO 14040/44 and addresses this growing demand,[22] for evaluating environmental impacts, including greenhouse gas emissions, water needs, acidification potential, eutrophication or particulate matter formation resulting from different materials and processes.[23] Implementing LCA for crustacean shell waste can identify environmental hotspots in chitin and chitosan processing and provide guidance for future optimization.

This work demonstrates the valorization of raw ocean waste into chitin, and its subsequent conversion to chitin nanocrystals through acid hydrolysis, or chitosan by deacetylation. Lobster and spider crab shells were used as source materials due to their limited attention by previous studies. Following isolation and physicochemical characterization, freestanding nanocomposite films composed exclusively of crustacean shell waste were produced by solvent casting. This strategy enables the fabrication of materials containing solely renewable carbon (from the biosphere), thereby avoiding the utilization of fossil carbon from the geosphere.[24] A clear benefit of these materials is their contribution toward defossilization, that is, utilizing solely renewable carbon, where the renewable carbon circulates between the biosphere, atmosphere, or technosphere to create a carbon circular economy. Furthermore, the optical, thermal and mechanical properties of the films demonstrate a reinforcing effect of the nanocrystals depending on their source. Additionally, the environmental impacts of chitin nanocrystal and chitosan valorization, as well as their subsequent processing into films, are quantified using life cycle assessment.

2. EXPERIMENTAL SECTION

2.1. Materials. Crustacean shells of lobster (*Homarus gammarus*) and spider crab (*M. squinado*) were purchased from a local store in San Sebastian. Hydrochloric acid (HCl, 37%), sodium hydroxide pellets (NaOH, ACS reagent) and formic acid (≥95%) was purchased from Sigma-Aldrich.

2.2. Chitin Nanocrystal and Chitosan Isolation. The chitin (Ch) was isolated from lobster shells ($Ch_{lobster}$) and spider crab (Ch_{crab}). First, demineralization was performed, which consisted of a 1 M HCl hydrolysis for 30 min at room temperature at a 1:15 (w/v) ratio. Second, the material was deproteinized using a 1 M NaOH treatment for 300 min at 85 °C at a 1:15 (w/v) ratio.[25] These two treatments were repeated again. At the end of each step, the solid was filtered and neutralized with distilled water. The obtained chitin was then used as a source material for chitin nanocrystal and chitosan fabrication. On the one hand, chitin nanocrystals from lobster ($ChNC_{lobster}$) and from spider crab ($ChNC_{crab}$) were isolated using an acid hydrolysis to remove the amorphous regions of chitin. For this aim, $Ch_{lobster}$ or Ch_{crab} was treated with 3 M HCl for 90 min at 100 °C at 1:30 (w/v) ratio. After that, the resulting solid was dispersed in distilled water and then washed by centrifugation. The sample was then dialyzed for 5 days with SpectraPor 12,000−14,000 molecular weight cutoff (MWCO) regenerated cellulose dialysis membranes (Spectrum Laboratories). Deionized water was changed every 12 h. The solid was filtered under pressure employing a 0.22 μm pore-size nylon filter and neutralized with distilled water. The two gel-like samples were finally stored in a refrigerator at 4 °C.[25] On the other hand, the chitin was deacetylated to obtain chitosan ($CS_{lobster}$ and CS_{crab}). To do so, chitin was treated using a 60% (v/v) NaOH solution for 240 min at 130 °C at 1:15 (w/v) ratio, under N_2 atmosphere. Finally, the solid was filtered and neutralized with distilled water.

2.3. Chitosan/ChNC Film Fabrication. Chitosan/ChNC films (CS/ChNC film) were prepared by solvent-casting. First, chitosan (1.5% w/v) was dissolved in a solution of formic acid (1.5% v/v) under constant stirring for 24 h at room temperature. Then, ChNC ($ChNC_{lobster}$ or $ChNC_{crab}$) were added at different 1 and 2% w/v. The solution was homogenized using an Ultra-Turrax (Heidolph Silent Crusher M., Germany) and bubbles were removed. Nine milliliters of the solution was casted onto polystyrene Petri dishes (50 mm in diameter) and was allowed to dry for 48 h.

2.4. Characterization. Fourier transform infrared (FTIR) spectroscopy analyses for isolated materials and fabricated films were performed using a PerkinElmer Spectrum Two using an attenuated total reflection (ATR) mode from Waltham (MA, USA). Spectra were collected after 64 scans in the range of 4000−600 cm^{-1} with a resolution of 4 cm^{-1}.

Solid-state carbon nuclear magnetic resonance (^{13}C NMR) was used for the acquisition of the spectra of Ch, CS, and ChNC, using a Bruker Avance III 400WBplus (Bruker, USA).[26] The degree of acetylation (DA %) was estimated according to[27]

$$\mathrm{DA}\ \% = \left[\frac{I_{CH_3}}{\frac{I_{C1}+I_{C2}+I_{C3}+I_{C4}+I_{C5}+I_{C6}}{6}}\right] \times 100 \quad (1)$$

where I_{CH_3} corresponds to the integral of the methyl carbon (CH_3), and I_{C1} to I_{C6} account for the integrals of the carbons of the D-glucopyranosyl ring from C1 to C6.

Powder X-ray diffraction (XRD) patterns of chitin, chitosan, and chitin nanocrystals were obtained by a Philip X'pert Pro (Phillips N.V., Amsterdam, Netherlands). Data was obtained at 2θ angles from 5 to 70° using Cu Kα radiation at 40 mA and 40 kV. The crystallinity index (CI %) was determined as

$$\mathrm{CI}\ \% = \left[\frac{I_{110} - I_{am}}{I_{110}}\right] \times 100 \quad (2)$$

where I_{110} corresponds to the maximum intensity (110) plane and I_{am} accounts for the amorphous diffraction (2θ = 12.5−13.5°).

https://doi.org/10.1021/acssuschemeng.4c01205
ACS Sustainable Chem. Eng. 2024, 12, 10363−10375

The thermal degradation behavior of isolated Ch, CS, and ChNC and produced films was studied by means of thermal gravimetric analysis (TGA/SDT 851 Mettler Toledo. Six milligrams of samples were heated from 25 to 800 °C at a rate of 10 °C·min^{-1} with a 20 mL·min^{-1} N_2 flow.

Atomic force microscope (AFM) was used to analyze the morphology and size features of chitin nanocrystals. AFM images were collected using a Dimension 3100 NanoScope IV (Veeco, USA). The images were scanned at room temperature using tapping mode with silicon nitride cantilever and 10 nm nominal radius tip at a frequency of 1 kHz. Samples of 3 × 3 cm^2 were utilized with AFM image dimensions of 5 × 5 μm^2 and 10 × 10 μm^2. To quantify the size of the nanocrystals (length and width), measurements have been taken at random locations on each sample and average values have been calculated with NanoScope Analysis 1.9 software.

The zeta-potential of water-dispersed ChNCs (0.02 mg·mL^{-1}) for pH values from 2 to 10 was determined using a Malvern Zetasizer Nano-ZS. The pH was adjusted by the addition of 0.1 M NaOH or 0.1 M HCl.

Films transparency was assessed by UV−vis transmission spectra with a V-730 (Jasco, Germany) spectrophotometer. Total transmittance experiments have been analyzed in the range of 200−800 nm with a sampling interval of 1 nm.

The thermal degradation behavior of CS/ChNC films was studied by means of thermal gravimetric analysis (Q50-0545, TA Instruments) in platinum pans at a heating rate of 10 °C·min^{-1} with a 60 mL·min^{-1} N_2 flow. The mechanical behavior of films was studied by uniaxial tensile tests using a vertical universal tensile tester (IDM MTC-100) equipped with a 500 N load cell at a deformation rate of 1 mm·min^{-1}. Specimens 50 mm long and 10 mm wide with thicknesses of 300 ± 60 μm were used. The mean average value and standard deviation Young's modulus (E) (0.5−1.5% strain region), stress and strain at yield (σ_y and ε_y, respectively), and stress and strain at break (σ_b and ε_b, respectively) were determined from five measurements.

To determine the moisture content (MC), the samples were cut into squares of 1 cm^2. Then, the samples were weighed and dried for 24 h at 106 °C (Memmert UN160 plus Twindisp, Germany). The MC was calculated as

$$\mathrm{MC}\ \% = \frac{W_0 - W_1}{W_1} \times 100 \tag{3}$$

where W_0 represents the weight before drying (g) and W_1 is the weight of the sample after drying (g). The samples were measured in triplicate and the result was reported as the mean and its standard deviation. The water contact angle (WCA) of the films was determined using a DataPhysiscs Oca20 (DataPhysics Instruments GmbH, Filderstadt, Germany) with the SCA20 software. At room temperature, drops of 5 μL distilled water were deposited onto film surfaces. Three replicates were performed for each sample. For density measurements, the films were cut into 1 cm^2 squares and the density was calculated by the ratio of film weight versus volume as

$$\mathrm{density} = \frac{W}{A\mathrm{Th}}\ (\mathrm{g/mm^3}) \tag{4}$$

where W is dry weight of the films (g), A is area (mm^2), and Th represents the thickness (mm). The measurements were performed in triplicate and the results are given as the average and standard deviation.

2.5. Life Cycle Assessment. Environmental impact studies were conducted using the life cycle assessment methodology in accordance with ISO 14040/44 standards.[29] For the sake of transparency and to facilitate future comparison, the life cycle inventory (LCI) of chitosan/ChNC isolation, and subsequent film processing is disclosed in Table 1. Additional process details can be found in Figure 1 (complete Life Cycle Inventory details are provided in Tables S1−S4 to enable future comparison). Briefly, the analysis considered the acquisition of raw materials, and the subsequent film processing, as well as all related upstream processes and the electricity for on-site production (cradle-to-gate boundaries) when performing the analysis.

Table 1. Material and Energy Input Inventory for Chitin (Ch), Chitosan (CS), Chitin Nanocrystals (ChNC), and Nanocomposite Films (CS/ChNC)

	material [unit]	Ch	CS	ChNC	CS/ChNC 1 wt %
inputs	shells [g]	100.00			
	Ch isolated from shells [g]		6.00	1.00	
	HCl (37%) [g]	65.66		3.31	
	NaOH (pellets, 99.9%) [g]	20.00	54.00		
	formic acid [g]				0.11
	deionized water [L]	26.39	6.90	2.00	0.06
	liquid N_2 [g]		90.00		
	water for cooling [L]	120.00		36.00	
	CS, dry basis [g]				0.99
	ChNC, dry basis [g]				0.01
	electricity [kW h]	4.09	2.03	1.73	0.30
outputs	HCl [g]	65.66		3.31	
	NaOH [g]	20.00	54.00		
	waste water (proteins, $CaCO_3$ dissolved) [L]	228.23	6.92	37.50	0.06
	formic acid [g]				0.11
	liquid N_2 [g]		90.00		
	Ch [g]	**18.30**			
	CS [g]		**3.93**		
	ChNC [g]			**0.89**	
	CS/ChNC film [g]				**1.00**

A medium voltage electricity source for Spanish grid is considered. The study also considered the amount of dissolved $CaCO_3$ and proteins as the main byproducts from the crustacean shells based on the theoretical composition of dried lobster (*H. gammarus*) (23.2 wt % protein, 38.2 wt % ash content, 20.3 wt % chitin).[19,20] To that end, the demineralization process was assumed to occur upon $CaCO_3$ decomposition into $CaCl_2$ and CO_2 as[28]

$$2\mathrm{HCl} + \mathrm{CaCO_3} \rightarrow \mathrm{CaCl_2} + \mathrm{H_2O} + \mathrm{CO_2}\uparrow \tag{5}$$

The environmental impacts were assessed using the OpenLCA 2.0.3 software and ecoinvent v3.9.1 database (released on December 2021) through a life cycle impact assessment. The ReCiPe 2016 Midpoint (H) methodology was used to obtain 18 environmental impact indicators. Although the study focused the global warming potential (GWP, kg·CO_2 equiv per kg of material), additional impact categories such as water consumption (m^3 per kg of material), freshwater ecotoxicity (kg of 1,4-DCB per kg of material), and terrestrial acidification (kg SO_2 equiv per kg of material) are also disclosed. Regarding the functional unit, the impacts are normalized to 1 kg of material (dry basis) using a mass allocation, as we understand this physical property results the most relevant characteristic to its future comparison.

3. RESULTS AND DISCUSSION

3.1. Chitin Nanocrystal and Chitosan Isolation. Attenuated total reflectance-Fourier transform infrared spectroscopy (ATR-FTIR) was used to characterize the isolated material. As displayed in Figure 2, chitin and ChNCs show transmission bands corresponding to the O−H and N−H stretching vibrations at about 3440 and 3260 cm^{-1}, respectively. In addition, the amide I, amide II and amide III bands were also observed around 1630, 1550 and 1310 cm^{-1}, respectively.[29] Further, peaks centered at 1378 and 1029 cm^{-1} arising from the CH_3 symmetrical deformation and C−O−C

https://doi.org/10.1021/acssuschemeng.4c01205
ACS Sustainable Chem. Eng. 2024, 12, 10363−10375

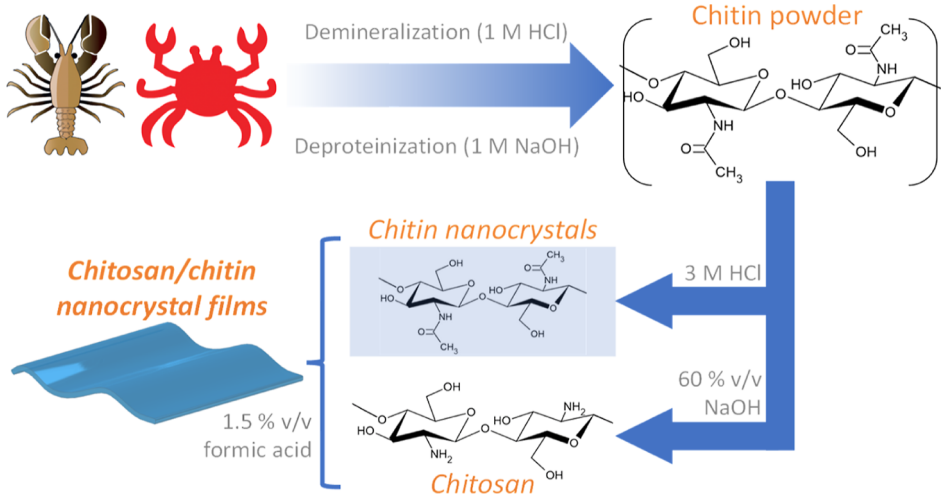

Figure 1. Scheme showing chitin, chitin nanocrystal, and chitosan isolation from crustacean shell wastes, and their subsequent processing into films.

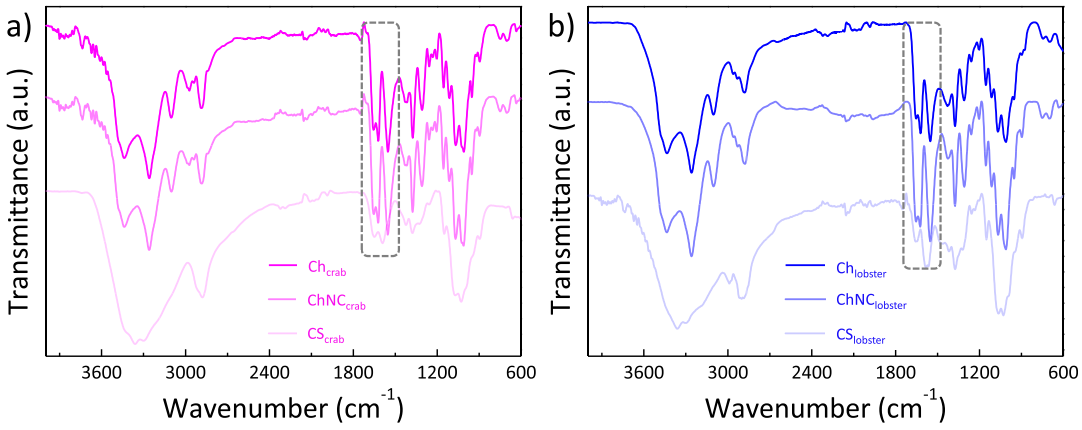

Figure 2. ATR-FTIR spectra of chitin (Ch), chitin nanocrystals (ChNC), and chitosan (CS) isolated from (a) spider crab and (b) lobster.

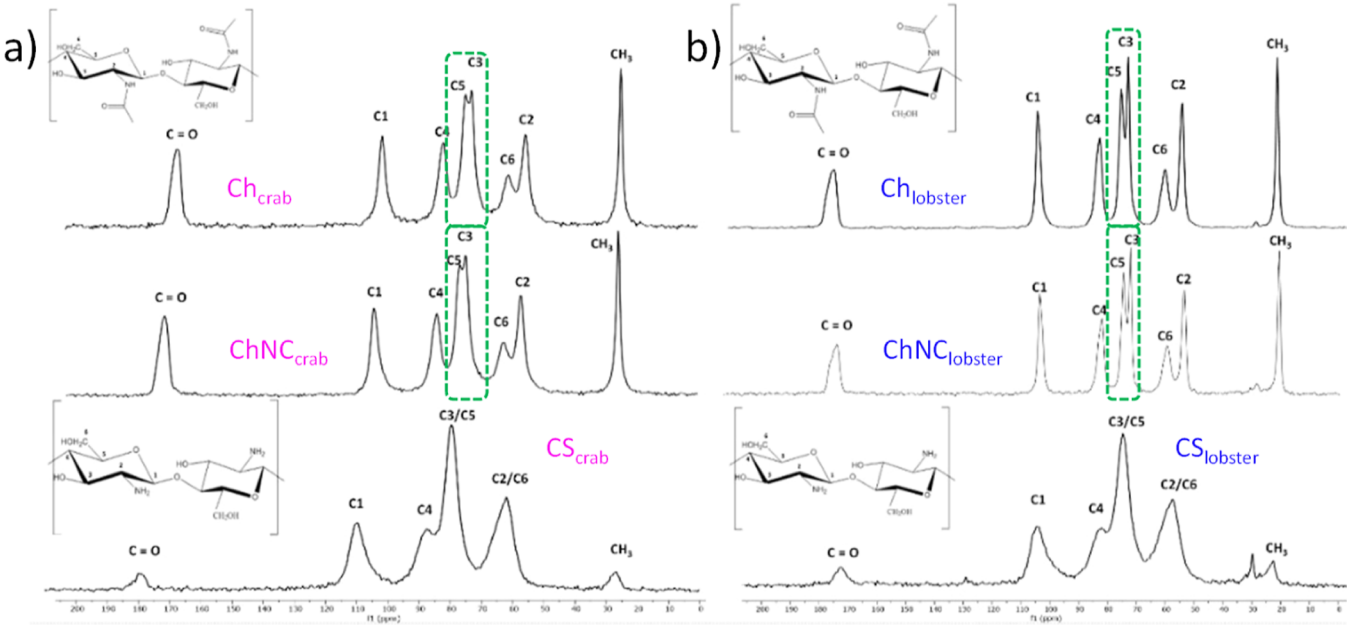

Figure 3. ^{13}C NMR spectra of Ch, ChNCs, and CS isolated from (a) spider crab and (b) lobster.

groups in chitin are also seen.[8] On the contrary, the chitosan spectra solely display the bands at 1645 and 1545 cm^{-1} corresponding to amide I and amide II, respectively. Besides, upon deacetylation of chitin, the band at 1655 cm^{-1} decreases

https://doi.org/10.1021/acssuschemeng.4c01205
ACS Sustainable Chem. Eng. 2024, 12, 10363−10375

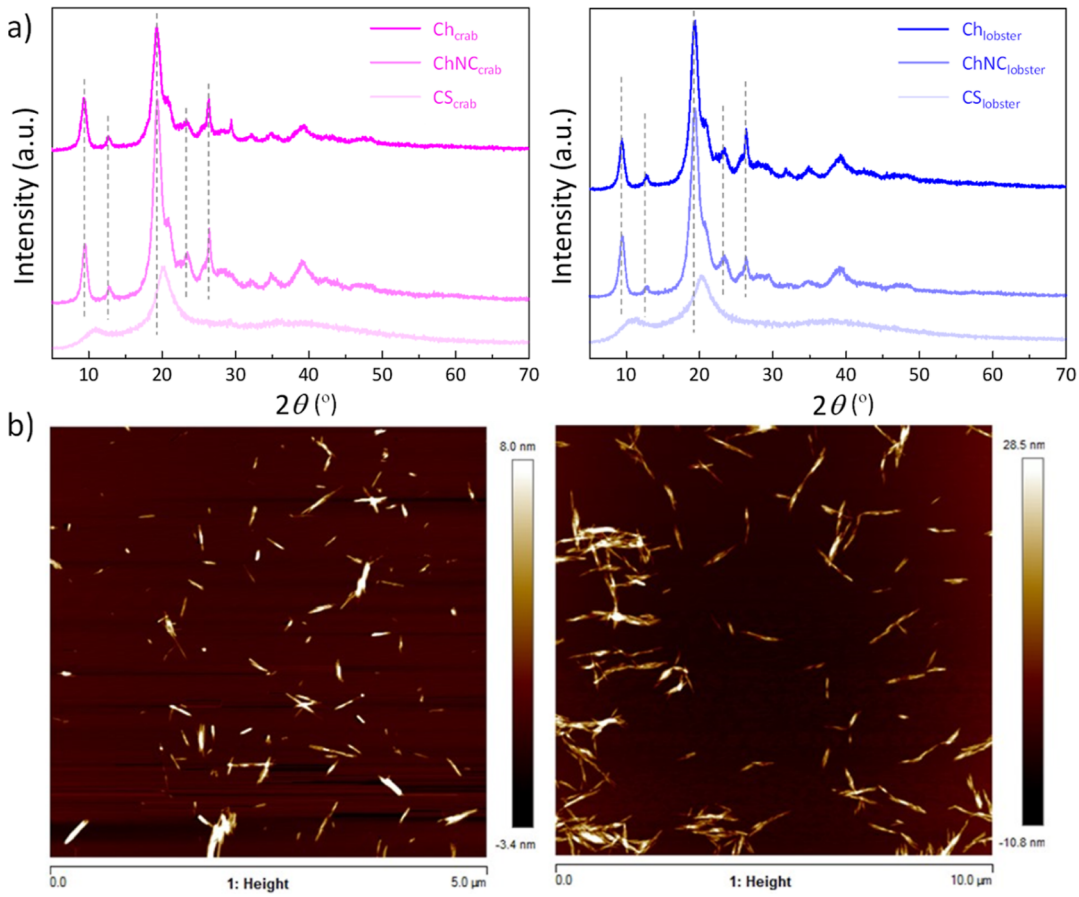

Figure 4. (a) XRD patterns of Ch, ChNCs, and CS isolated from spider crab (left) and lobster (right); (b) contact-mode AFM height images of isolated ChNCs from spider crab (left) and lobster (right).

while the band at 1545 cm^{-1} increases, indicating the prevalence of NH_2 groups.[30] In addition, the C−H stretching vibration has also been observed at 1400 cm^{-1}.

^{13}C NMR was applied to obtain further insights on the conformational characteristics of isolated material. Figure 3 summarizes the ^{13}C NMR spectra of isolated materials from crab and lobster sources. All the samples present the signal corresponding to the methyl group (CH_3) at around 20 ppm and the carbonyl group (C═O) at 170 ppm. The large intensity of the CH_3 signals for Ch and ChNCs over the weak signal observed for CS suggest that high degree of acetylation values have been achieved.[30] In addition, the signal from the D-glucopyranosyl ring is observed between 55 and 105 ppm as indicated by the C2, C6, C4, and C1 signals. Interestingly, a doublet (green highlighted) is observed at C5 and C3 for Ch and ChNC samples (70−75 ppm), while these signals appear overlapped for CS. The DA values extracted from these spectra (eq 1) very similar values for ChNCs extracted from both sources (94.7% for $ChNC_{lobster}$ and 93.0% for $ChNC_{crab}$) in line with literature. On the contrary, very low DA values of 13.3 and 10.9% are obtained for CS extracted from lobster and spider crab, respectively. Such high degree of acetylation for Ch and ChNCs, and low values for CS, prove the suitability of lobster and spider crab to isolate high purity chitinuous biomass. Finally, no traces of protein could be observed (C−O at 180 ppm, C−N at 55 ppm),[27] proving the suitability of lobster and spider crab to render neat chitinuous biomass.

The crystal structure of isolated materials was studied by XRD. As depicted in Figure 4a, the diffraction patterns barely change depending on the source material (lobster of spider crab shells) and are characteristic of a of a semicrystalline material, with well distinguishable crystalline peaks overlapped with an amorphous domain. Ch and ChNCs present well-defined diffraction peaks centered at 2θ = 9.3, 12.7, 19.3, 23.3, and 26.3°.[31] These peaks can be identified with native α-chitin (similarly to previous reports on ChNCs isolated upon acid hydrolysis),[18,32,33] having a orthorhombic cell structure and large degree of acetylation for Ch and correlate to the crystalline planes of (020), (021), (110), (130), and (013), respectively.[30,34] The crystallinity index was obtained through the peak height method, which accounts for the intensity ratios between the intensity of the most crystalline reflection (110) with the intensity of the diffuse halo according to eq 2. Results show an increase from the 87.8−89.4% for Ch, to 90.1−92.2% to ChNCs (in line with the intensity increase observed), underlying the removal of the amorphous regions upon HCl hydrolysis. On the contrary, CS solely presents two broad diffraction peaks corresponding to the (020) and (110) planes and located at 2θ = 11.0 and 20.4°. Reduced crystallinities over Ch and ChNC are obtained (59.0 and 74.8% for lobster- and crab-derived CS, respectively) due to the disruption of H-bonding upon deacetylation.[35] This material amorphization for CS quantified by XRD correlates well with the degree of acetylation estimated by ^{13}C NMR.[36]

The morphology of ChNC was observed by atomic force microscopy (AFM). AFM images in Figure 4b show the occurrence of well-dispersed nanoparticles as a result of the excellent colloidal stability of ChNCs in aqueous solutions.[18]

https://doi.org/10.1021/acssuschemeng.4c01205
ACS Sustainable Chem. Eng. 2024, 12, 10363−10375

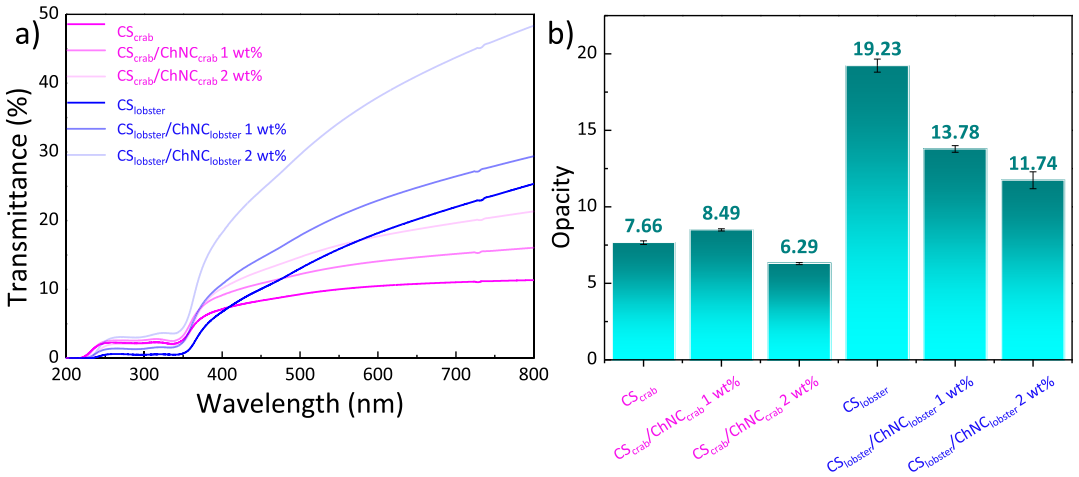

Figure 5. (a) UV−vis transmittance spectra and (b) opacity values of CS/ChNC nanocomposite films.

As expected, both ChNCs exhibited a rod-like morphology being longer for $ChNC_{lobster}$. In fact, the $ChNC_{lobster}$ showed lengths and diameters of 550 ± 37 and 57 ± 5 nm, while $ChNC_{crab}$ presented dimensions of 407 ± 29 nm and width 50 ± 3 nm. As a result, the aspect ratio varied between 9.7 for $ChNC_{lobster}$ and 8.1 for $ChNC_{crab}$. Such lengths results are in the upper range of literature values for nanochitin isolated from crustacean exoskeletons utilizing chemical hydrolysis top-down isolation procedures,[18,27,31,37,38] where the Ch hydrolysis at the glycosidic bond with hydrogen ions from HCl dissociation yields nanoparticles having lengths that remain between 110 and 560 nm and widths of 40−60 nm when isolated from shrimp or crab shells. In particular, Phongying et al. obtained needle-shaped nanocrystals having a length of 200−560 nm and a width between 18 and 40 nm (shrimp shells treated at 3 M HCl for 105 °C and 3 h),[37] while rod-shaped chitin nanocrystals from shrimp and lobster shells have been reported to present lengths of 300−390 nm and widths of around 42−60 nm,[25,27] or the ChNCs having particle sizes of 200−600 nm isolated from crab shells by acid hydrolysis.[32] The surface charge of water-dispersed $ChNC_{crab}$ $ChNC_{lobster}$ has been determined by zeta-potential measurements. Figure S1 reveals a positive net charge at low pH values for both nanochitins due to protonation of the *N*-acetyl groups of chitin. As the pH increases, the nanoparticles get continuously (negatively) charged from the starting +31.8 and +29.9 mV to reach an isoelectric point of pH 6.7 for $ChNC_{crab}$ and 7.2 for $ChNC_{lobster}$, respectively, matching literature observations.[18,30]

Besides, the thermogravimetric analysis (TGA) curves of isolated Ch, CS, and ChNCs are shown in Figure S2. Two major mass losses are observed for all the samples. The first thermodegradation event comprises around 5−8% mass loss and occurred around 100 °C due to the evaporation of physically adsorbed and hydrogen-bonded water. ChNCs adsorb more water (by weight) in comparison with Ch and CS, in line with recent results.[30] Then, the second mass loss is attributed to the degradation and dehydration of the polysaccharide backbone and the decomposition of the acetylated or deacetylated units.[29,39] Finally, dehydration and deoxygenation of residual polymeric chains occur to yield a residual carbon of ∼40 wt % for ChNCs 20−35 wt % at 700 °C.[36] Importantly, the second event from the degradation of 2-amino-2-deoxy-D-glucopyranose units in Ch occurs at temperatures of 300−460 °C, while it is lowered to 280−400 °C for CS and to 250−350 °C for ChNCs. The reduced thermal stability of CS and ChNCs compared to their parent Ch is explained in terms of differences in hydrogen bonding between carbonyl group (C═O) to $-NH_2$ groups and $-CH_2OH$ groups in the side chain.[40] Besides, the chitinous biomass isolated from lobster shells degrades at lower temperatures over the material obtained from spider crab shells, probably due to small differences in the degree of acetylation, crystallinity degree and morphology.

3.2. Film Properties. Crack-free and homogeneous freestanding CS films were fabricated by solvent-casting upon CS dissolution in 1.5% v/v formic acid and biocolloid dispersion using an Ultra-Turrax. Formic acid has been selected because it is the simplest organic acid, it has a widespread use in the industry (chemical, agricultural, textile, pharmaceutical, and agro-food), it is relatively sustainable, noncorrosive, and has antifungal properties. Moreover, both formic acid and its formate ion degrade easily in seawater.[41] Although a Schiff's base may be produced when using formic acid due to its lower pK_a value over acetic acid, the concentration used was sufficiently small to avoid undesired secondary reactions with the aldehyde.

The films reinforced by ChNCs are entirely obtained from lobster or spider crab endocuticles. Although the casting of the chitosan/formic acid solution and subsequent drying for 48 h to remove solvent is not preferable for industrial application, this solvent casting approach continues being the major manufacturing approach at laboratory scale. Alternatives to reduce manufacturing time include electrospraying,[42] ionic gelation,[43] spin coating,[44] or exploiting the already existing papermaking procedures.[45] In any case, the solvent casting approach is adequate for fundamental science purposes as it enables the preparation of well-dispersed nanocomposites at low material quantities. The macroscopic appearance of the films is shown in Figure S3, where diameters above 50 mm are obtained. The curled and shrunk aspect of the films arises from drying-induced capillary forces originating from increased water−air surface area, causing tensile stresses in the films.[46] The films presented a yellowish tone, and shift from slightly opaque to translucent after ChNC incorporation. The yellow tone is often observed then chitosan is treated in alkaline solutions at temperatures above 100 °C, and is due to a Maillard reaction between the amino and carbonyl groups.[47] Therefore, future work should focus on shortening chitosan

https://doi.org/10.1021/acssuschemeng.4c01205
ACS Sustainable Chem. Eng. 2024, 12, 10363−10375

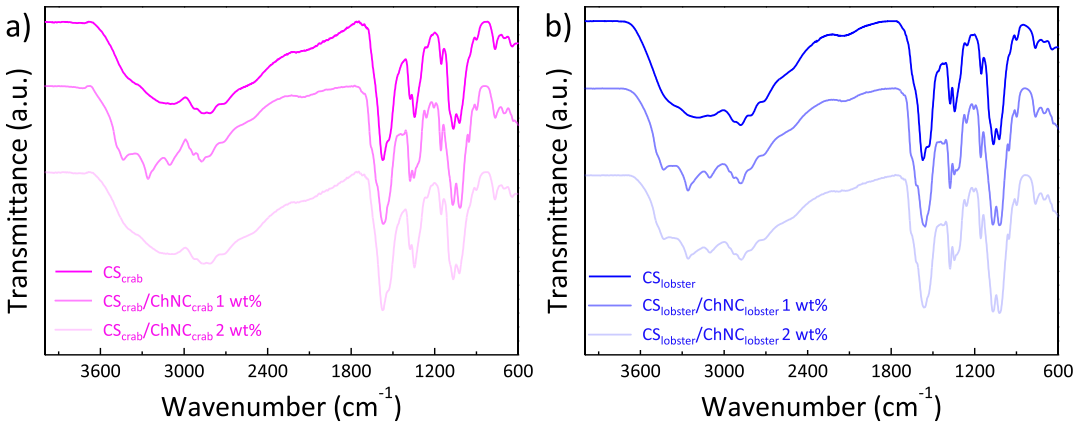

Figure 6. ATR-FTIR spectra of CS/ChNC nanocomposite films derived from (a) spider crab and (b) lobster.

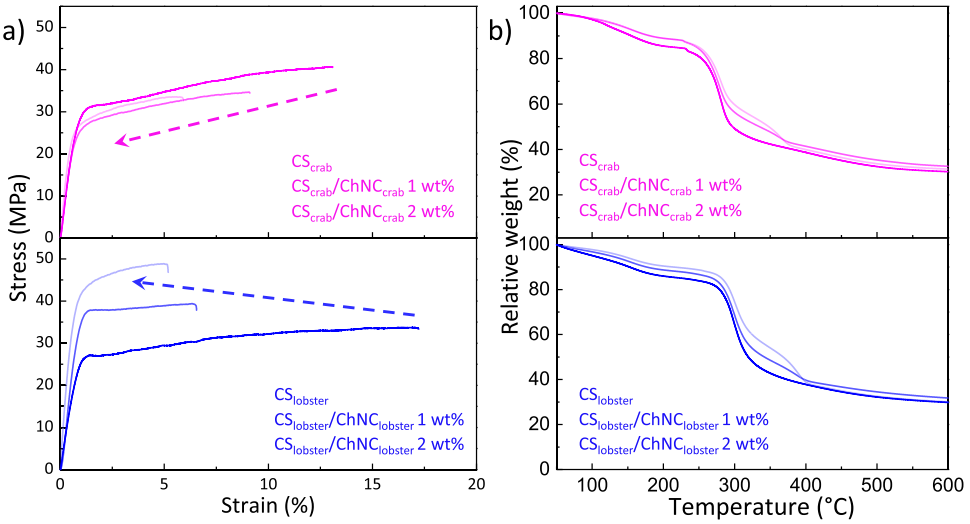

Figure 7. (a) Representative stress−strain curves of CS/ChNC films isolated from spider crab (top) and lobster exoskeletons (bottom). The arrows indicate the trend upon ChNC incorporation. (b) Thermogravimetric curves of CS/ChNC films from spider crab (top) and lobster exoskeletons (bottom).

reaction times, using nonconcentrated alkaline solutions, and lowering reaction temperatures. The optical properties were further studied by ultraviolet−visible (UV−vis) spectroscopy in transmittance mode for the λ = 200−800 nm region and the results are shown in Figure 5a,b. The films exhibit intermediate transmittance values in the visible region together with strongly opaque behavior in the UV region. Neat Ch$_{lobster}$ and Ch$_{crab}$ films offer UV-blocking efficiencies of 99 and 96% in the UV-C region, while keeping optical transparencies of ∼15 and ∼10% in the visible region, respectively. It is interesting to note that the incorporation of ChNCs leads to a systematic increase in transmitted light. This transmittance increase is due to the dense packing of nanochitin with its host CS, limiting the occurrence of cavities in the cast film that cause undesired light scattering.[48] Besides, a homogeneous dispersion of the nanochitin within the CS host with no aggregation avoids Rayleigh scattering effects. The addition of ChNC results in increased transparency, making it suitable for developing coatings or food-packaging films that require optical transparency. The film opacity at λ = 600 nm can be obtained from these spectra according to[49]

$$\text{opacity} = \frac{A_{600}}{L} \tag{6}$$

where A_{600} corresponds to the absorbance at wavelength of 600 nm and L is film thickness in mm. The films derived from lobster exhibit reduced opacities, with values of 7.84 ± 0.06 and 19.49 ± 0.20 for neat Ch$_{lobster}$ and Ch$_{crab}$, respectively (Figure 5a,b). In agreement with UV−vis results, the addition of ChNCs notable decreases opacity, indicating the potential of isolated nanochitin to enhance the optical appearance of biobased materials.

Besides, the occurrence of specific interactions between composite constituents has been investigated by ATR-FTIR. As depicted in Figure 6, all the samples present the CS around 3440 and 3290 cm^{-1} assigned as O−H and N−H stretching vibration, respectively, together with the amide II band at ∼1565 cm^{-1}.[50] The presence of ChNCs in the films is evidenced by the two peaks at 1376 and 1370 cm^{-1} originating from the CH methyl groups of Ch.[29]

One of the main motivations for this work is to obtain freestanding films with improved mechanical performance at relatively low environmental cost. In this context, alternative choices for nanochitin isolation exist, such as chitin nanofibrils (ChNFs), which could be isolated through simple disintegration of native chitin utilizing mechanical treatments without the removal of the disordered and noncrystalline regions. A priori, ChNFs may present reduced environmental impacts

https://doi.org/10.1021/acssuschemeng.4c01205
ACS Sustainable Chem. Eng. 2024, 12, 10363−10375

Table 2. Tensile Testing Parameters as a Function of ChNC Loading[a]

source	wt %	E (MPa)	ε_y (%)	σ_y (MPa)	ε_b (%)	σ_b (MPa)
spider crab	0	3390 ± 1160	1.6 ± 0.1	33.8 ± 13.4	13.0 ± 1.9	41.6 ± 16.9
	1	3770 ± 810	N. O.	N. O.	9.1 ± 1.4	30.7 ± 5.7
	2	4220 ± 870	N. O.	N. O.	6.1 ± 1.8	29.8 ± 4.4
lobster	0	2270 ± 690	2.1 ± 0.3	26.8 ± 5.2	17.2 ± 3.7	31.4 ± 4.7
	1	3520 ± 520	2.0 ± 0.4	35.9 ± 6.6	6.4 ± 3.0	38.2 ± 7.5
	2	5530 ± 830	N. O.	N. O.	5.1 ± 0.9	47.4 ± 7.7

[a]E: Young's modulus; ε_y: elongation at yield; σ_y: stress at yield; ε_b: elongation at break; σ_b: stress at break. N. O.: not observed.

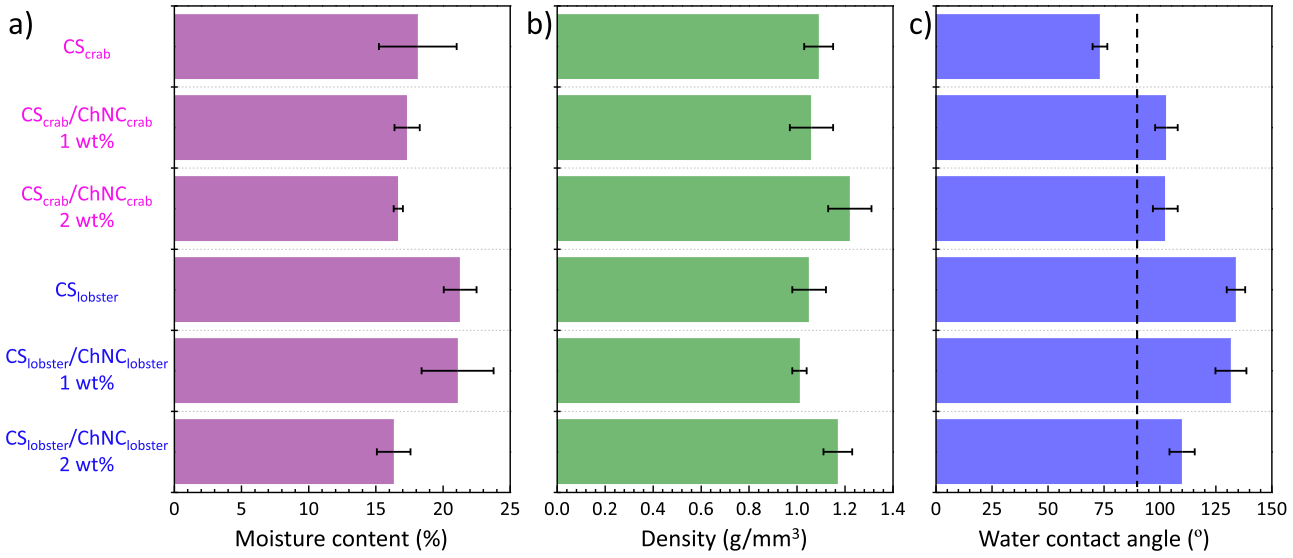

Figure 8. (a) Moisture content, (b) density, and (c) water contact angle of fabricated CS/ChNC films. The dashed line shows the transition from hydrophilic (values below 90°) to hydrophobic.

(per mass of material) over ChNCs as extensive chemical treatments are circumvented. Nevertheless, such simpler mechanical treatments often yield highly flexible ChNFs with heterogeneously distributed lateral dimensions,[8] resulting in materials suitable for hydrogel formation (physical entanglements are achieved at low concentrations), but with reduced mechanical reinforcing effects. Accordingly, this work utilizes ChNCs rather than ChNFs to mechanically reinforce chitosan films. In this context, uniaxial tensile tests were conducted on CS/ChNC nanocomposite films under constant strain rate and the results are disclosed in Figure 7a (average values over five specimens are reported). Besides, Table 2 summarizes the Young's modulus (E), tensile stress and elongation at yield (σ_y, ε_y), and tensile stress elongation at break (σ_b, ε_b). The neat CS films exhibit a semiductile behavior with modulus values of 2270 ± 690 and 3390 ± 1160 MPa for the material sources from lobster and spider crab, respectively, and elongations at break exceeding 10%. Yield values for both materials are close to 2% for elongation, and 30 MPa for stress. These values remain higher than those reported in the literature,[49,51,52] indicating a good balance between stiffness and ductility provided by the CS isolated from lobster and spider crab exoskeleton valorization.

ChNC incorporation increases Young's modulus and tensile strength values at expenses of ductility, where break is obtained before yield. On particular note is the E increase in the CS$_{lobster}$/ChNC$_{lobster}$ system, where the addition of 2 wt % nanochitin enhances the modulus up to 5530 ± 830 MPa. This modulus increase may originate from the high electronegativity of the O in the −OH groups, which facilitates the formation of H-bonds (and other interactions, including ionic) with the cationic amino/acetamido groups in chitosan,[53] as well as the spindle-shaped crystalline nature of the nanochitin that efficiently reinforces the matrix. In this sense, it should be noted that ChNC$_{lobster}$ incorporation yields notable increases in tensile strength values (from 31.4 ± 4.7 to 47.4 ± 7.7 MPa with 2 wt %), while the presence of 2 wt % ChNC$_{crab}$ reduces the stress at break by 28%. This behavior indicates that nanochitin having larger aspect ratios (9.7 vs 8.1 for ChNC$_{lobster}$ and ChNC$_{crab}$, respectively) results more efficient in improving the mechanical properties (a similar trend is also observed in terms of Young's modulus).

Overall, an effective mechanical reinforcement of nanochitin into CS is achieved. This is in contrast to other biopolymer nanocomposite systems where the incorporation of fillers reduces Young's modulus due to weakened bonding (e.g., carrageenan/anthocyanin/curcumin,[54] CS/deacetylated Ch nanofibers).[55] It is important to note that the mechanical performance of the nanocomposite materials remains well above the modulus and ductility shown by conventional thermoplastics such as polybutylene succinate or poly(L-lactide), whose modulus hardly goes beyond 2500 MPa and elongation at break is found below 10%.[56] Besides, the observed embrittlement is a common feature in polymer nanocomposites, where a premature fracture is observed due to stress concentration effects at filler-rich regions.[57]

The TGA curves of CS/ChNC nanocomposite films at different ChNC concentrations are shown in Figure 7b. The chitosan derived from lobster shows an increased stability against thermodegradation events as indicated by the ∼30 °C

https://doi.org/10.1021/acssuschemeng.4c01205
ACS Sustainable Chem. Eng. 2024, 12, 10363−10375

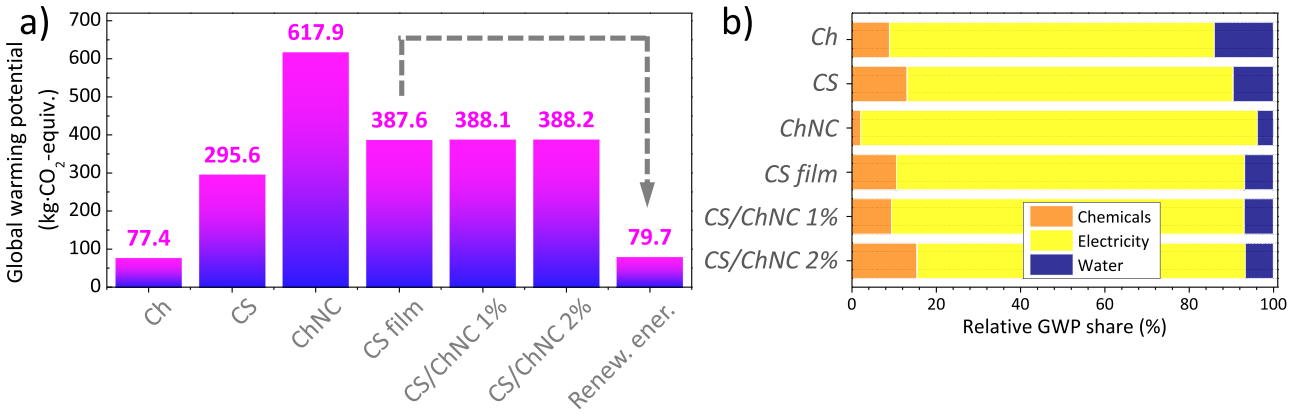

Figure 9. (a) GWP of chitin, chitosan, and ChNC raw materials together with the films (a medium voltage electricity from the Spanish grid is considered). The arrow indicates the predicted GWP for a chitosan film processed using renewable energy. Impacts are normalized to 1 kg of material. (b) Relative GWP distribution for raw materials and films.

shift toward higher temperatures on the weight loss. Besides, the addition of ChNCs to neat CS films delays thermodegradation by further 8 °C. Specifically, the onset of thermal degradation, accounted as the temperature at which the first 20 wt % loss is obtained, increases from 259 to 264 °C after the inclusion of 2 wt % ChNCs for crab-derived materials (292–301 °C for lobster-derived materials). This enhanced thermodegradation stability is consistent with previous observations for natural rubber,[58] or dental resin adhesives.[59] This delay is attributable to the high surface area of nanochitin, which acts as an effective barrier to the permeation of combustion gases.[60] Notably, the thermal stability increase is even greater when $ChNC_{lobster}$ is added because of its larger aspect ratio of 9.7 versus 8.1 for $ChNC_{crab}$, which offers enhanced gas barrier properties in polymer nanocomposite films.[61] Importantly, this behavior is opposite to the catalyzing effect of sulfated cellulose nanocrystals when incorporated into polymeric matrices,[62] highlighting the potential of nanochitin as an additive to enhance the thermal stability of polymeric matrices.

Additionally, the moisture content, density, and water contact angle of CS/ChNC films have been analyzed to provide insights toward the use of these materials in food packaging applications (Figure 8). The moisture content of the neat chitosan films, 18.1 ± 2.9 and 21.3 ± 1.2% for CS_{crab} and $CS_{lobster}$, respectively, matches literature,[63] and decreases upon the incorporation of nanochitin. On the contrary, the film density is increased from values around 1.07 $g{\cdot}cm^{-3}$ for neat films, to 1.19 $g{\cdot}cm^{-3}$ for the 2 wt % nanocomposite counterparts because of the increased packing of highly crystalline ChNCs with larger densities. Finally, the introduction of ChNCs into chitosan results in a differential effect. Crab-derived materials transition from hydrophilic to hydrophobic upon ChNC incorporation as denoted by the water contact angle (WCA) increase from 73.2 ± 3.3 to 102.4 ± 5.6°. This behavior results adequate for packaging uses, were reducing the contact with water is advantageous.[63] Contrarily, lobster-derived materials exhibiting a reduction in hydrophobicity. This affinity toward water may also explain the differential behavior in tensile strength obtained upon ChNC incorporation in Figure 7a, where an increased WCA is correlated with a plasticizing effect of ambient water in the mechanical behavior (i.e., reduced tensile strength from 41.6 ± 16.9 to 29.8 ± 4.4 MPa for crab-derived nanocomposites).[64] On the contrary, a reduced WCA is translated into a stiffening effect of the material, increasing the tensile strength from 31.4 ± 4.7 to 47.4 ± 7.7 MPa.

3.3. Environmental Impact Assessment. To identify environmental hotspots during CS/ChNC film production we applied a cradle-to-gate life cycle assessment using 1 kg of material (dry basis) as the functional unit.[17,65,66] Note that although the experiments were conducted from 100 g of dry shells, the functional unit of 1 kg enables comparison with benchmark materials, for which impacts are typically provided in reference to a kilo, regardless of the reaction scale. To facilitate cross-comparison with literature data on chitinuous film production, the global warming potential (GWP, measured as CO_2 equivalent emissions) impact indicator is first reported in Figure 9a. Considering raw material requirements, chemical treatments and electricity consumption, chitin could be isolated with a CO_2 footprint of 77.4 kg CO_2 $equiv{\cdot}kg^{-1}$. The 0.3 and 4.4 kg CO_2 $equiv{\cdot}kg^{-1}$ obtained for commercialized lignocellulosic materials such as cellulose fiber (from postconsumer paper) and carboxymethyl cellulose (processing of alkaline cellulose with mono acetic acid), respectively (ecoinvent v3.9, ReCiPe 2016 Midpoint H) demonstrate that the current chitin isolation from crustaceans has a notable environmental cost. A possible alternative toward low-environmental impact chitin results the utilization of alternative sources where chitin does not coexist with $CaCO_3$, thus avoiding the need for demineralization procedures using HCl. In this context, fungi are emerging a promising feedstock for chitin, where short mechanical treatments assisted by mild alkali processing are sufficient.[66]

Besides, the increased need for chemicals and electricity results in GWP values for CS and ChNCs of 295.6 and 617.9 kg CO_2 $equiv{\cdot}kg^{-1}$, respectively. These values remain in the lower-range regarding the greenhouse gas emissions of 543.5–906.8 kg CO_2 $equiv{\cdot}kg^{-1}$ reported by Berroci et al. for ChNCs isolated from crab and shrimp shells,[66] or the 810.7 kg CO_2 $equiv{\cdot}kg^{-1}$ shown by nanofibrillated cellulose,[67] indicating the environmental soundness of the process developed here. From the other side, with values ranging from 387.6 to 388.2 kg CO_2 $equiv{\cdot}kg^{-1}$, intermediate impacts between raw CS and ChNCs are obtained for the production of free-standing CS/ChNC film. The higher impact compared to raw CS is attributed to the additional use of formic acid, water and electricity for film processing.

https://doi.org/10.1021/acssuschemeng.4c01205
ACS Sustainable Chem. Eng. 2024, 12, 10363–10375

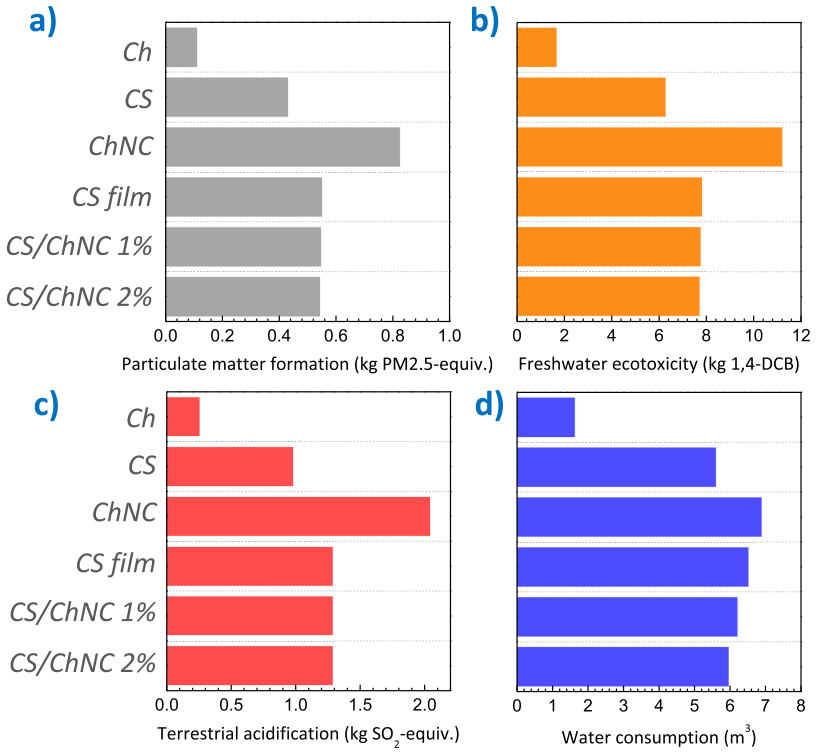

Figure 10. Environmental impacts during the isolation of chitin, chitosan, and ChNC, and chitosan/ChNC nanocomposite film processing, for the categories of: (a) particulate matter formation; (b) freshwater ecotoxicity; (c) terrestrial acidification and (d) water consumption. A medium voltage electricity from the Spanish grid is considered.

Figure 9b displays the relative contribution of chemical use, electricity consumption, and water needs to the GWP impact category. For all materials considered here, the greenhouse gas emissions are largely driven by electricity consumption, which accounts for 77 to 94% depending on the isolated material. As a general trend, the energy contribution increases with process intensity. In other words, CS, and especially ChNCs and CS/ChNC films, require additional synthetic steps (long hydrolysis treatments or dissolution/dispersion steps), which increases the energy use. In this context, we simulated a possible reduction in the environmental impact of neat chitosan film production upon transitioning from the current fossil-based electricity mix to a 100% renewable energy mix. The GWP of the sensitivity analysis (considering a renewable energy grid) performed is shown in Figure 9a, with a significant reduction from 387.6 to 79.7 kg CO_2 equiv·kg^{-1} for a neat CS film (79.8 kg CO_2 equiv·kg^{-1} for the CS/ChNC 2 wt % film). This drop is in line with recent observations by Hao et al. quantifying the environmental impact of large-scale cellulose nanocrystal production,[68] who pointed that regions with abundant low-carbon energy produce materials with well-reduced greenhouse gas emissions (for cellulose nanocrystals, the impact vary between 13 and 800 kg CO_2 equiv·kg^{-1} depending on the electricity source). Importantly, the GWP of 77.4 kg CO_2 equiv·kg^{-1} is very close to the ∼77 kg CO_2 equiv·kg^{-1} recently reported by Riofrio et al. for 1 kg of CS production from shrimp shells for a plant with an annual processing capacity of 5000 tons (European fossil-based energy was used during their analyses).[65]

As summarized in Figure 10 and Tables S5 and S6, a similar trend is observed for the impact categories of particulate matter formation, freshwater ecotoxicity, terrestrial acidification and water consumption. In general, a 6-fold and 9-fold increase is observed for CS and ChNCs in comparison with Ch. Specifically, water consumption significantly increases from 1.64 to 5.61 m^3, and to 6.89 m^3, for Ch, CS, ChNCs, respectively. Although such water need remains below literature data for ChNCs isolated from shrimp and crab shells (21.44 and 14.15 m^3, respectively), future works should address the extensive washing and purification steps required during chitin and chitosan isolation so a reduced water consumption could be obtained. As a matter of fact, we utilized 23.75 L of water for chitin purification, 6 L for chitosan washing, and 1.5 L for ChNC neutralization (1 L dialysis, 0.4 L centrifuge, 0.1 L filtering). Furthermore, it should be noted that the use of 100% renewable energy during production simultaneously reduces the freshwater ecotoxicity, and terrestrial acidification of chitosan film production from 7.8 to 3.8 kg 1,4-DCB, and from 1.29 to 0.27 kg SO_2 equiv·kg^{-1}, respectively. However, the impact category of water consumption increases notably from 6.5 to 21.0 m^3 due to hydropower generation, indicating the need for careful design of an optimized process with attention to different environmental impact categories (and not only greenhouse gas emissions). In any case, this study demonstrates the suitability of lobster and crab exoskeletons, especially when renewable energy sources are implemented during processing, to obtain renewable materials with competitive environmental performance.

Although this work is focused on the chitin isolation from underutilized crustacean shell wastes, integrated biorefineries converting biomass into chitin and additional coproducts (e.g., proteins, fats, astaxanthin, $CaCO_3$) should be pursued in the near future to enhance feedstock utilization and optimize the energy/material use of the isolation processes. In this regard, proteins could be utilized for human or animal feed, fats could

https://doi.org/10.1021/acssuschemeng.4c01205
ACS Sustainable Chem. Eng. 2024, 12, 10363−10375

be employed as feedstock for biogas production, $CaCO_3$ could be applied in construction, and astaxanthin could be utilized in cosmetics. For example, the protein-rich effluent generated during chitin isolation could be treated using a solid−liquid extraction process at room temperature and ambient pressure with acetone, ethanol or acetic acid.[69] Regarding environmental impact calculations, in multioutput processes such as this, attributional LCA calculations subtract the environmental burdens of obtained coproducts from the whole process, as the need for new isolation procedures (proteins and others) is displaced. Conversely, an allocation approach (a physical parameter such as mass, economic value, or causal) could be used to account for the environmental impacts for each of the coproducts.[70] The two approaches offer significant reductions in environmental impact, thus indicating that biorefinery integration is a viable option.

4. CONCLUSIONS

This work investigates the potential for valorization of novel chitinous feedstock from renewable carbon. Lobster and spider crab shells are used as important chitin sources. The chitinous biorefinery proposed in this study leaded to the production of ChNCs with lengths of 550 ± 37 and 407 ± 29 nm for $ChNC_{lobster}$ and $ChNC_{crab}$, respectively. The biocolloids exhibited the characteristic features of α-chitin crystal structure, with varying crystallinity degrees ranging from 92.2% for $ChNC_{lobster}$ to 90.1% for $ChNC_{crab}$. Additionally, high degrees of acetylation of 94.7 and 93.0% were obtained, respectively. Besides, the raw Ch was treated to obtain CS having a notably low degree of acetylation of 10.9 and 13.3% for lobster and crab sources, respectively. This CS achieved a low crystallinity degree of 59.0 and 74.8% for both sources, subsequently. Combining the products obtained, outstanding CS/ChNC films were fabricated from lobster and spider crab by solvent-casting. The thermodegradation onset temperatures of the films were increased by ∼8 °C due to the incorporation of ChNCs. Besides, a good UV/vis shielding of the films was achieved, with reduced opacity values for chitosan/$ChNC_{lobster}$. All formulations displayed a semiductile character, where the incorporation of ChNC significantly enhanced the Young's modulus of the materials, making them competitive against petroleum-based polymers. Additionally, this work disclosed the environmental impacts of $ChNC_{lobster}$ and $CS_{lobster}$ isolation, as well as the fabrication of CS/$ChNC_{lobster}$ nanocomposite film based on a life cycle assessment. These processes generated a CO_2 footprint ranging from 77.4 to 617.9 kg CO_2 equiv kg^{-1}, most of which was due to energy requirements. Importantly, the transition to a low carbon energy mix could potentially reduce the GWP of CS/ChNC films to 79.8 kg CO_2 equiv kg^{-1}. With these thermal, optical and mechanical properties, this work demonstrated the potential of chitinous sources derived from renewable carbon feedstock for the development of sustainable bioproducts with competitive functional performance against fossil-based materials and boost the implementation of a carbon circular economy.

■ ASSOCIATED CONTENT

Data Availability Statement

All the data used to support the findings of this study are included within the article.

Supporting Information

The Supporting Information is available free of charge at https://pubs.acs.org/doi/10.1021/acssuschemeng.4c01205.

Thermogravimetric traces of the isolated material and optical micrograph of the films. Tables showing the environmental impacts of obtained materials grouped into 18 impact categories (PDF)

■ AUTHOR INFORMATION

Corresponding Authors

Jalel Labidi − *Biorefinery Processes Research Group, Chemical and Environmental Engineering Department, Engineering Faculty of Gipuzkoa, University of the Basque Country UPV/EHU, 20018 Donostia, Spain*; Email: jalel.labidi@ehu.eus

Erlantz Lizundia − *Life Cycle Thinking Group, Department of Graphic Design and Engineering Projects, Faculty of Engineering in Bilbao, University of the Basque Country (UPV/EHU), 48013 Bilbao, Spain; BCMaterials, Basque Center for Materials, Applications and Nanostructures, 48940 Leioa, Spain;* orcid.org/0000-0003-4013-2721; Email: erlantz.liizundia@ehu.eus

Authors

Rut Fernández-Marín − *Biorefinery Processes Research Group, Chemical and Environmental Engineering Department, Engineering Faculty of Gipuzkoa, University of the Basque Country UPV/EHU, 20018 Donostia, Spain*

Amaia Morales − *Biorefinery Processes Research Group, Chemical and Environmental Engineering Department, Engineering Faculty of Gipuzkoa, University of the Basque Country UPV/EHU, 20018 Donostia, Spain*

Xabier Erdocia − *Biorefinery Processes Research Group, Department of Applied Mathematics, University of the Basque Country UPV/EHU, 48013 Bilbao, Spain;* orcid.org/0000-0001-7780-876X

Maider Iturrondobeitia − *Life Cycle Thinking Group, Department of Graphic Design and Engineering Projects, Faculty of Engineering in Bilbao, University of the Basque Country (UPV/EHU), 48013 Bilbao, Spain*

Complete contact information is available at: https://pubs.acs.org/10.1021/acssuschemeng.4c01205

Author Contributions

The manuscript was written through contributions of all authors. All authors have given approval to the final version of the manuscript.

Notes

The authors declare no competing financial interest.

■ ACKNOWLEDGMENTS

Financial support from the "2021 Euskampus Missions 1.0. Programme" granted by Euskampus Fundazioa is acknowledged. The authors are thankful for funds from the University of the Basque Country (GIU21/010). Technical and human support provided by SGIker (UPV/EHU, MICINN, GV/EJ, EGEF, and ESF) is gratefully acknowledged.

■ REFERENCES

(1) Cabernard, L.; Pfister, S.; Oberschelp, C.; Hellweg, S. Growing Environmental Footprint of Plastics Driven by Coal Combustion. *Nat. Sustain.* **2022**, *5* (2), 139−148.

(2) Lebreton, L.; Andrady, A. Future Scenarios of Global Plastic Waste Generation and Disposal. *Palgrave Commun.* **2019**, *5* (1), 6.
(3) Seddon, N.; Chausson, A.; Berry, P.; Girardin, C. A. J.; Smith, A.; Turner, B. Understanding the Value and Limits of Nature-Based Solutions to Climate Change and Other Global Challenges. *Philos. Trans. R. Soc., B* **2020**, *375* (1794), 20190120.
(4) OECD. *Global Plastics Outlook*, 2022 (accessed Feb, 2024).
(5) Tardy, B. L.; Richardson, J. J.; Greca, L. G.; Guo, J.; Bras, J.; Rojas, O. J. Advancing Bio-Based Materials for Sustainable Solutions to Food Packaging. *Nat. Sustain.* **2023**, *6* (4), 360−367.
(6) Lizundia, E. Competitive and Environmentally Sustainable Bioproducts: Mild Top-Down Processing of Biomass to Renewable Carbon. *ACS Sustain. Resour. Manag.* **2024**, *1* (5), 813−815.
(7) Lizundia, E.; Kundu, D. Advances in Natural Biopolymer-Based Electrolytes and Separators for Battery Applications. *Adv. Funct. Mater.* **2021**, *31* (3), 2005646.
(8) Bai, L.; Liu, L.; Esquivel, M.; Tardy, B. L.; Huan, S.; Niu, X.; Liu, S.; Yang, G.; Fan, Y.; Rojas, O. J. Nanochitin: Chemistry, Structure, Assembly, and Applications. *Chem. Rev.* **2022**, *122* (13), 11604−11674.
(9) Li, T.; Chen, C.; Brozena, A. H.; Zhu, J. Y.; Xu, L.; Driemeier, C.; Dai, J.; Rojas, O. J.; Isogai, A.; Wågberg, L.; Hu, L. Developing Fibrillated Cellulose as a Sustainable Technological Material. *Nature* **2021**, *590* (7844), 47−56.
(10) Jin, T.; Liu, T.; Lam, E.; Moores, A. Chitin and Chitosan on the Nanoscale. *Nanoscale Horiz.* **2021**, *6* (7), 505−542.
(11) Lizundia, E.; Nguyen, T.-D.; Winnick, R. J.; MacLachlan, M. J. Biomimetic Photonic Materials Derived from Chitin and Chitosan. *J. Mater. Chem. C* **2021**, *9* (3), 796−817.
(12) Ling, S.; Kaplan, D. L.; Buehler, M. J. Nanofibrils in Nature and Materials Engineering. *Nat. Rev. Mater.* **2018**, *3* (4), 18016.
(13) Dufresne, A. Polysaccharide Nano Crystal Reinforced Nanocomposites. *Can. J. Chem.* **2008**, *86* (6), 484−494.
(14) Ji, Y.; Waters, S.; Lim, E.; Lang, A. W.; Ciesielski, P. N.; Shofner, M. L.; Reynolds, J. R.; Meredith, J. C. Minimizing Oxygen Permeability in Chitin/Cellulose Nanomaterial Coatings by Tuning Chitin Deacetylation. *ACS Sustain. Chem. Eng.* **2022**, *10* (1), 124−133.
(15) Ruiz, D.; Michel, V. F.; Niederberger, M.; Lizundia, E. Chitin Nanofibrils from Fungi for Hierarchical Gel Polymer Electrolytes for Transient Zinc-Ion Batteries with Stable Zn Electrodeposition. *Small* **2023**, *19* (45), 2303394.
(16) Chen, C.; Wu, Q.; Wan, Z.; Yang, Q.; Xu, Z.; Li, D.; Jin, Y.; Rojas, O. J. Mildly Processed Chitin Used in One-Component Drinking Straws and Single Use Materials: Strength, Biodegradability and Recyclability. *Chem. Eng. J.* **2022**, *442*, 136173.
(17) Greca, L. G.; Azpiazu, A.; Reyes, G.; Rojas, O. J.; Tardy, B. L.; Lizundia, E. Chitin-Based Pulps: Structure-Property Relationships and Environmental Sustainability. *Carbohydr. Polym.* **2024**, *325*, 121561.
(18) Narkevicius, A.; Steiner, L. M.; Parker, R. M.; Ogawa, Y.; Frka-Petesic, B.; Vignolini, S. Controlling the Self-Assembly Behavior of Aqueous Chitin Nanocrystal Suspensions. *Biomacromolecules* **2019**, *20* (7), 2830−2838.
(19) Toliba, A. O.; Rabie, M. A.; El-Araby, G. M. Extending the Shelf-Life of Cold Stored Strawberry by Chitosan and Carnauba Coatings. *Zagazig J. Agric. Res.* **2014**, *41* (5), 1067−1076.
(20) Pires, C.; Marques, A.; Carvalho, M. L.; Batista, I. Chemical Characterization of Cancer Pagurus, Maja Squinado, Necora Puber and Carcinus Maenas Shells. *Poult. Fish Wildl. Sci.* **2017**, *5* (1), 181.
(21) Lizundia, E.; Luzi, F.; Puglia, D. Organic Waste Valorisation towards Circular and Sustainable Biocomposites. *Green Chem.* **2022**, *24* (14), 5429−5459.
(22) Laurent, A.; Weidema, B. P.; Bare, J.; Liao, X.; Maia de Souza, D.; Pizzol, M.; Sala, S.; Schreiber, H.; Thonemann, N.; Verones, F. Methodological Review and Detailed Guidance for the Life Cycle Interpretation Phase. *J. Ind. Ecol.* **2020**, *24* (5), 986−1003.
(23) Iturrondobeitia, M.; Vallejo, C.; Berroci, M.; Akizu-Gardoki, O.; Minguez, R.; Lizundia, E. Environmental Impact Assessment of $LiNi_{1/3}Mn_{1/3}Co_{1/3}O_2$ Hydrometallurgical Cathode Recycling from Spent Lithium-Ion Batteries. *ACS Sustain. Chem. Eng.* **2022**, *10* (30), 9798−9810.
(24) *Renewable Carbon Initiative*; Nova-Institut GmbH, 2022. https://renewable-carbon.eu/news/higher-price-increases-for-fossils-nova-price-indices-for-fossil-resources-metals-and-biomass-1980-2021/ (accessed May, 2024).
(25) Salaberria, A. M.; Labidi, J.; Fernandes, S. C. M. Chitin Nanocrystals and Nanofibers as Nano-Sized Fillers into Thermoplastic Starch-Based Biocomposites Processed by Melt-Mixing. *Chem. Eng. J.* **2014**, *256*, 356−364.
(26) Kasaai, M. R. Determination of the Degree of N-Acetylation for Chitin and Chitosan by Various NMR Spectroscopy Techniques: A Review. *Carbohydr. Polym.* **2010**, *79* (4), 801−810.
(27) Fernández-Marín, R.; Hernández-Ramos, F.; Salaberria, A. M.; Andrés, M. Á.; Labidi, J.; Fernandes, S. C. M. Eco-Friendly Isolation and Characterization of Nanochitin from Different Origins by Microwave Irradiation: Optimization Using Response Surface Methodology. *Int. J. Biol. Macromol.* **2021**, *186*, 218−226.
(28) Santos, V. P.; Marques, N. S. S.; Maia, P. C. S. V.; Lima, M. A.; Franco, L. D.; Campos-Takaki, G. M. Seafood Waste as Attractive Source of Chitin and Chitosan Production and Their Applications. *Int. J. Mol. Sci.* **2020**, *21* (12), 4290.
(29) Cao, S.-L.; Gu, W.-M.; Ou-Yang, W.-D.; Chen, D.-C.; Yang, B.-Y.; Lai, L.-H.; Wu, Y.-D.; Liu, Y.-J.; Zhu, J.; Chen, W.-J.; Gai, Z.-Q.; Hou, X.-D.; Ma, Y.-Z.; An, Y.-X. Preparation, Characterization and Application of Rod-like Chitin Nanocrystal by Using p-Toluenesulfonic Acid/Choline Chloride Deep Eutectic Solvent as a Hydrolytic Media. *Carbohydr. Polym.* **2019**, *213*, 304−310.
(30) Larrañaga, A.; Bello-Álvarez, C.; Lizundia, E. Cytotoxicity and Inflammatory Effects of Chitin Nanofibrils Isolated from Fungi. *Biomacromolecules* **2023**, *24* (12), 5737.
(31) Magnani, C.; Fazilati, M.; Kádár, R.; Idström, A.; Evenäs, L.; Raquez, J.-M.; Lo Re, G. Green Topochemical Esterification Effects on the Supramolecular Structure of Chitin Nanocrystals: Implications for Highly Stable Pickering Emulsions. *ACS Appl. Nano Mater.* **2022**, *5* (4), 4731−4743.
(32) Liu, H.; Feng, Y.; Cao, X.; Luo, B.; Liu, M. Chitin Nanocrystals as an Eco-Friendly and Strong Anisotropic Adhesive. *ACS Appl. Mater. Interfaces* **2021**, *13* (9), 11356−11368.
(33) Su, X.; Wan, Z.; Lu, Y.; Rojas, O. Control of the Colloidal and Adsorption Behaviors of Chitin Nanocrystals and an Oppositely Charged Surfactant at Solid, Liquid, and Gas Interfaces. *Langmuir* **2024**, *40* (9), 4881−4892.
(34) Isobe, N.; Kaku, Y.; Okada, S.; Kawada, S.; Tanaka, K.; Fujiwara, Y.; Nakajima, R.; Bissessur, D.; Chen, C. Identification of Chitin Allomorphs in Poorly Crystalline Samples Based on the Complexation with Ethylenediamine. *Biomacromolecules* **2022**, *23* (10), 4220−4229.
(35) Facchinatto, W. M.; Santos, D. M. d.; Fiamingo, A.; Bernardes-Filho, R.; Campana-Filho, S. P.; Azevedo, E. R. d.; Colnago, L. A. Evaluation of Chitosan Crystallinity: A High-Resolution Solid-State NMR Spectroscopy Approach. *Carbohydr. Polym.* **2020**, *250*, 116891.
(36) Santos, M.; Del Carlo, O.; Hong, J.; Liu, Z.; Jiang, S.; Hrapovic, S.; Lam, E.; Jin, T.; Moores, A. Effect of Surface Functionality on the Rheological and Self-Assembly Properties of Chitin and Chitosan Nanocrystals and Use in Biopolymer Films. *Biomacromolecules* **2023**, *24* (9), 4180−4189.
(37) Phongying, S.; Aiba, S.; Chirachanchai, S. Direct Chitosan Nanoscaffold Formation via Chitin Whiskers. *Polymer* **2007**, *48* (1), 393−400.
(38) Yu, Z.; Ji, Y.; Meredith, J. C. Multilayer Chitin-Chitosan-Cellulose Barrier Coatings on Poly(Ethylene Terephthalate). *ACS Appl. Polym. Mater.* **2022**, *4* (10), 7182−7190.
(39) Kaya, M.; Sargin, I.; Tozak, K. O.···; Baran, T.; Erdogan, S.; Sezen, G. Chitin Extraction and Characterization from Daphnia Magna Resting Eggs. *Int. J. Biol. Macromol.* **2013**, *61*, 459−464.
(40) Rahman, M. M.; Maniruzzaman, M. A New Route of Production of the Meso-Porous Chitosan with Well-Organized Honeycomb Surface Microstructure from Shrimp Waste without

Destroying the Original Structure of Native Shells: Extraction, Modification and Characterization Study. *Results Eng.* **2023**, *19*, 101362.
(41) Bulushev, D. A.; Ross, J. R. H. Towards Sustainable Production of Formic Acid. *ChemSusChem* **2018**, *11* (5), 821−836.
(42) Liu, Y.; Wang, S.; Lan, W. Fabrication of Antibacterial Chitosan-PVA Blended Film Using Electrospray Technique for Food Packaging Applications. *Int. J. Biol. Macromol.* **2018**, *107*, 848−854.
(43) Wei, Z.; Pan, P.; Hong, F. F.; Cao, Z.; Ji, Y.; Chen, L. A Novel Approach for Efficient Fabrication of Chitosan Nanoparticles-Embedded Bacterial Nanocellulose Conduits. *Carbohydr. Polym.* **2021**, *264*, 118002.
(44) Do, P.; Doan, T. U.; Tran, T.; Hoang, D.; Pham, K. N. The Effect of Content and Thickness of Chitosan Thin Films on Resistive Switching Characteristics. *Sci. Technol. Dev. J.* **2020**, *23* (3), 632−639.
(45) Song, Z.; Li, G.; Guan, F.; Liu, W. Application of Chitin/Chitosan and Their Derivatives in the Papermaking Industry. *Polymers* **2018**, *10* (4), 389.
(46) Karna, N. K.; Wohlert, J.; Hjorth, A.; Theliander, H. Capillary Forces Exerted by a Water Bridge on Cellulose Nanocrystals: The Effect of an External Electric Field. *Phys. Chem. Chem. Phys.* **2023**, *25* (8), 6326−6332.
(47) Szymańska, E.; Winnicka, K. Stability of Chitosan—A Challenge for Pharmaceutical and Biomedical Applications. *Mar. Drugs* **2015**, *13* (4), 1819−1846.
(48) Ifuku, S.; Ikuta, A.; Egusa, M.; Kaminaka, H.; Izawa, H.; Morimoto, M.; Saimoto, H. Preparation of High-Strength Transparent Chitosan Film Reinforced with Surface-Deacetylated Chitin Nanofibers. *Carbohydr. Polym.* **2013**, *98* (1), 1198−1202.
(49) Fernández-Marín, R.; Fernandes, S. C. M.; Sánchez, M. Á. A.; Labidi, J. Halochromic and Antioxidant Capacity of Smart Films of Chitosan/Chitin Nanocrystals with Curcuma Oil and Anthocyanins. *Food Hydrocoll.* **2022**, *123*, 107119.
(50) Lin, N.; Zhao, S.; Gan, L.; Chang, P. R.; Xia, T.; Huang, J. Preparation of Fungus-Derived Chitin Nanocrystals and Their Dispersion Stability Evaluation in Aqueous Media. *Carbohydr. Polym.* **2017**, *173*, 610−618.
(51) Rodrigues, C.; de Mello, J. M. M.; Dalcanton, F.; Macuvele, D. L. P.; Padoin, N.; Fiori, M. A.; Soares, C.; Riella, H. G. Mechanical, Thermal and Antimicrobial Properties of Chitosan-Based-Nanocomposite with Potential Applications for Food Packaging. *J. Polym. Environ.* **2020**, *28* (4), 1216−1236.
(52) Mujtaba, M.; Fernández-Marín, R.; Robles, E.; Labidi, J.; Yilmaz, B. A.; Nefzi, H. Understanding the Effects of Copolymerized Cellulose Nanofibers and Diatomite Nanocomposite on Blend Chitosan Films. *Carbohydr. Polym.* **2021**, *271*, 118424.
(53) Gal, M. R.; Rahmaninia, M.; Hubbe, M. A. A Comprehensive Review of Chitosan Applications in Paper Science and Technologies. *Carbohydr. Polym.* **2023**, *309*, 120665.
(54) Zhou, X.; Yu, X.; Xie, F.; Fan, Y.; Xu, X.; Qi, J.; Xiong, G.; Gao, X.; Zhang, F. PH-Responsive Double-Layer Indicator Films Based on Konjac Glucomannan/Camellia Oil and Carrageenan/Anthocyanin/Curcumin for Monitoring Meat Freshness. *Food Hydrocoll.* **2021**, *118*, 106695.
(55) Li, Y.; Ying, Y.; Zhou, Y.; Ge, Y.; Yuan, C.; Wu, C.; Hu, Y. A PH-Indicating Intelligent Packaging Composed of Chitosan-Purple Potato Extractions Strength by Surface-Deacetylated Chitin Nanofibers. *Int. J. Biol. Macromol.* **2019**, *127*, 376−384.
(56) Rincón-Iglesias, M.; Salado, M.; Lanceros-Mendez, S.; Lizundia, E. Magnetically Active Nanocomposites Based on Biodegradable Polylactide, Polycaprolactone, Polybutylene Succinate and Polybutylene Adipate Terephthalate. *Polymer* **2022**, *249*, 124804.
(57) Liu, A.; Berglund, L. A. Fire-Retardant and Ductile Clay Nanopaper Biocomposites Based on Montmorrilonite in Matrix of Cellulose Nanofibers and Carboxymethyl Cellulose. *Eur. Polym. J.* **2013**, *49* (4), 940−949.
(58) Liu, Y.; Liu, M.; Yang, S.; Luo, B.; Zhou, C. Liquid Crystalline Behaviors of Chitin Nanocrystals and Their Reinforcing Effect on Natural Rubber. *ACS Sustain. Chem. Eng.* **2018**, *6* (1), 325−336.
(59) D'Acierno, F.; Liu, L.; Nguyen, T.-D.; Michal, C. A.; Palma-Dibb, R. G.; Carvalho, R. M.; MacLachlan, M. J. Physical and Mechanical Properties of a Dental Resin Adhesive Containing Hydrophobic Chitin Nanocrystals. *Dent. Mater.* **2022**, *38* (12), 1855−1865.
(60) Zhang, Q.; Wang, Y. C.; Bailey, C. G.; Yuen, R. K. K.; Parkin, J.; Yang, W.; Valles, C. Quantifying Effects of Graphene Nanoplatelets on Slowing down Combustion of Epoxy Composites. *Composites, Part B* **2018**, *146*, 76−87.
(61) Mandal, S.; Roy, D.; Mukhopadhyay, K.; Dwivedi, M.; Joshi, M. Mechanistic Insight into the Role of the Aspect Ratio of Nanofillers in the Gas Barrier Properties of Polymer Nanocomposite Thin Films. *RSC Appl. Interfaces* **2024**.
(62) Wu, H.; Liu, X.; Hua, X.; Zhang, J. Thermal-Oxidation Degradation of Polylactic Acid/Cellulose Nanocrystal Composites: Effects of Surface Chemistry. *Ind. Crops Prod.* **2023**, *202*, 117008.
(63) Mohammed, K.; Yu, D.; Mahdi, A. A.; Zhang, L.; Obadi, M.; Al-Ansi, W.; Xia, W. Influence of Cellulose Viscosity on the Physical, Mechanical, and Barrier Properties of the Chitosan-Based Films. *Int. J. Biol. Macromol.* **2024**, *259*, 129383.
(64) Mali, S.; Sakanaka, L. S.; Yamashita, F.; Grossmann, M. V. E. Water Sorption and Mechanical Properties of Cassava Starch Films and Their Relation to Plasticizing Effect. *Carbohydr. Polym.* **2005**, *60* (3), 283−289.
(65) Riofrio, A.; Alcivar, T.; Baykara, H. Environmental and Economic Viability of Chitosan Production in Guayas-Ecuador: A Robust Investment and Life Cycle Analysis. *ACS Omega* **2021**, *6* (36), 23038−23051.
(66) Berroci, M.; Vallejo, C.; Lizundia, E. Environmental Impact Assessment of Chitin Nanofibril and Nanocrystal Isolation from Fungi, Shrimp Shells and Crab Shells. *ACS Sustain. Chem. Eng.* **2022**, *10* (43), 14280−14293.
(67) Turk, J.; Oven, P.; Poljanšek, I.; Lešek, A.; Knez, F.; Malovrh Rebec, K. Evaluation of an Environmental Profile Comparison for Nanocellulose Production and Supply Chain by Applying Different Life Cycle Assessment Methods. *J. Clean. Prod.* **2020**, *247*, 119107.
(68) Hao, Z.; Hamad, W. Y.; Yaseneva, P. Understanding the Environmental Impacts of Large-Scale Cellulose Nanocrystals Production: Case Studies in Regions Dependent on Renewable and Fossil Fuel Energy Sources. *Chem. Eng. J.* **2023**, *478*, 147160.
(69) Vicente, F. A.; Ventura, S. P. M.; Passos, H.; Dias, A. C. R. V.; Torres-Acosta, M. A.; Novak, U.; Likozar, B. Crustacean Waste Biorefinery as a Sustainable Cost-Effective Business Model. *Chem. Eng. J.* **2022**, *442*, 135937.
(70) Provost-Savard, A.; Majeau-Bettez, G. Substitution Modeling Can Coherently Be Used in Attributional Life Cycle Assessments. *J. Ind. Ecol.* **2024**, *28*, 410−425.

https://doi.org/10.1021/acssuschemeng.4c01205
ACS Sustainable Chem. Eng. 2024, 12, 10363−10375